Reproducibility in Joint Blind Source Separation: Application to fMRI Analysis

Francisco Laport* †, Trung Vu †, Hanlu Yang †, Vince Calhoun ‡ and Tülay Adali †
† Department of Computer Science and Electrical Engineering, University of Maryland Baltimore County, MD, 21250, USA
* CITIC Research Center, University of A Coruña, 15008 A Coruña, Spain
‡Tri-Institutional Center for Translational Research in Neuroimaging and
Data Science (TReNDS), Georgia State University, Georgia Institute of Technology, and
Emory University, Atlanta, GA 30303, USA
Email: *francisco.laport@udc.es, †{flopez2, trungvv, hyang3, adali}@umbc.edu, ‡ vcalhoun@gsu.edu

2023 57th Asilomar Conference on Signals, Systems, and Computers | 979-8-3503-2574-4/23/$31.00 ©2023 IEEE | DOI: 10.1109/IEEECONF59524.2023.10477028

***Abstract*—Joint blind source separation (JBSS) techniques have been successfully applied for the analysis of multi-subject functional magnetic resonance imaging (fMRI) data. However, convergence in JBSS can be only guaranteed to a local optimum, since typically cost functions are non-convex. Also, iterative methods are usually implemented with random initialization for best performance, resulting in high variability, especially for more flexible solutions. Yet, the assessment of the reproducibility of JBSS has been limited in the literature, even though it has been demonstrated that when not taken into account, the solutions can be highly suboptimal. In this work, we propose a framework for the evaluation of the reproducibility of independent vector analysis, an important JBSS solution. We introduce a mechanism for selecting the model complexity that offers the most consistent and accurate solution, and demonstrate results to underline its importance using resting state fMRI data.**

***Index Terms*—joint blind source separation, independent vector analysis, reproducibility, fMRI analysis.**

I. Introduction

During the last few years, the scientific community has witnessed an increase in the availability of shared neuroimaging data [1]. This higher accessibility to datasets has promoted the development of large-scale and multi-subject analysis for understanding the brain function and the identification of brain disorders [2]. Functional magnetic resonance imaging (fMRI) and the study of brain functional connectivity patterns have proved to be an effective technique for the identification of biomarkers in various disorders such as schizophrenia, bipolar disorder and autism [3].

Data-driven methods and, in particular, blind source separation (BSS) techniques, such as independent component analysis (ICA), have been widely applied for the study of fMRI data [2], [4]. These methods assume that there are linear combinations of latent variables of interest in the observed data and apply a matrix decomposition solution for their extraction. For fMRI data, ICA decomposes the brain activities of a subject into maximally independent functional networks. It provides a fully interpretable result, where the rows/columns of the decomposed factors can be associated with the spatially independent sources and their corresponding time courses [2], [5]. To leverage the joint information across multi-subject data, a joint analysis must be performed. Joint BSS (JBSS) techniques, such as group ICA (GICA) [6], generalizes ICA to multiple datasets and exploits the dependencies across them [7]. However, since GICA assumes a common subspace for all the subjects, it might lead to information loss and to limited capture of inter-subject variability [5], [8]. Independent vector analysis (IVA) extends ICA to multiple datasets. It exploits the statistical dependencies across datasets through a multivariate density model to achieve a powerful decomposition [5], [7], [9]. IVA has proved to be an effective technique for preserving inter-subject variability in the fMRI analysis [10]. However, IVA is computationally expensive and its performance degrades as the number of datasets increases [11]. In this regard, constrained IVA (cIVA) incorporates prior knowledge to the analysis to improve the performance of IVA in large-scale multi-subjects datasets [11], [12].

Although JBSS techniques have played an important role in the analysis of practical problems, the assessment of their computational reproducibility has been limited [13], [14]. Considering that the cost functions of most JBSS algorithms are non-convex, convergence can only be guaranteed to a local optimum. Iterative methods are usually implemented since closed-form solutions do not exist for these problems. In addition, as there is no unique and perfect initialization for these problems, taking the best solution among those obtained by multiple random initializations has proved to be effective [13]–[15]. Hence, even though all the algorithmic quantities are fixed, the obtained results can be quite different due to the variability introduced by the initialization. Furthermore, the complexity of the model and its order plays an important role in the quality of the estimates and its stability. Different model orders will lead to different solutions to the problem. The proper selection of the model order is an important feature in model match. A good model match that accurately captures the properties of the observed data leads to better interpretability. Also, most reproducible solutions are shown to lead to results with better interpretability [13], [14].

It is important to highlight that due to the bias and variance dilemma in estimation theory, a highly reproducible solution

This work is supported in part by the grants NIH R01MH118695, NIH R01MH123610, NIH R01AG073949, NSF 2316420, and Xunta de Galicia – Fulbright ED481B 2022/012

with reduced variability might lack of enough flexibility to capture all the informative features of the data and yield a high bias, and vice versa. In this regard, cIVA introduces reliable prior information to the analysis which guides the algorithms to avoid a sub-optimal solution, hence, achieving a good balance between bias and variance even when used in conjunction with a flexible approach.

The evaluation of the performance of an algorithm can be a difficult problem in practical cases where the ground truth is unknown. Cross-ISI, a global metric inspired by inter-symbol interference (ISI), measures the consistency of the results across different runs and it can be computed when there is no ground truth since it only depends on the estimated demixing matrix [15]. According to the bias-variance dilemma, a highly consistent result does not guarantee a low bias in the estimates and, as introduced by the nonparametric, prediction, activation, influence, reproducibility, and resampling (NPAIRS) framework in neuroimaging [16], both accuracy and reproducibility should be taken into account in algorithm performance. In practical problems where the ground truth is unknown, the estimation of the accuracy can be a difficult task. Towards this end, in this work, we propose a normalized measure related to the cost function that is evaluated to guide the selection of the model order. For IVA, which maximizes the independence of the latent source component vectors, mutual information is a natural cost function. Nevertheless, in contrast to other matrix decomposition methods with a straightforward distance-based metric (e.g., nonnegative matrix factorization (NMF) or sparse decomposition), the evaluation of the IVA cost function is nontrivial. For instance, the selection of different nonlinearities changes the cost values. Therefore, a metric associated with the goal of the algorithm, such as the pairwise normalized mutual information among the estimated sources, can be applied together with cross-ISI for the selection of the best result.

In this paper, we evaluate the computational reproducibility of JBSS techniques with a practical focus where there is no ground truth. In addition, we propose a new mechanism for selecting the best model order based on cross-ISI and the pairwise normalized mutual information among the estimated sources to guarantee the selection of the most consistent and accurate result. We also demonstrate that our solution provides replicable results and more interpretable functional networks when applied to resting state fMRI data of 98 subjects. The rest of this paper is organized as follows. Section II provides a brief overview of the JBSS problem. Then, the employed methods are described in Section III, and Section IV presents the results obtained when the proposed mechanism is applied to real fMRI data.

II. JBSS PROBLEM FORMULATION

Consider K datasets $\boldsymbol{x}^{[k]}(v) \in \mathbb{R}^N$ composed by V samples ($v = 1 \dots V$) and where each dataset $\boldsymbol{x}^{[k]}(v) = [\boldsymbol{x}_1^{[k]}(v), \dots, \boldsymbol{x}_N^{[k]}(v)] \in \mathbb{R}^N$ is modeled as a linear mixture of N latent sources $\boldsymbol{s}^{[k]}(v) = [\boldsymbol{s}_1^{[k]}(v), \dots, \boldsymbol{s}_N^{[k]}(v)] \in \mathbb{R}^N, 1 \leq k \leq K$. Then, the JBSS generative model is defined as

$$\boldsymbol{x}^{[k]}(v) = \boldsymbol{A}^{[k]} \boldsymbol{s}^{[k]}(v), \tag{1}$$

where $\boldsymbol{A}^{[k]}$ is an invertible mixing matrix. JBSS techniques estimate K demixing matrices $\boldsymbol{W}^{[k]}$ to compute the source estimates $\boldsymbol{y}^{[k]}(v) = [\boldsymbol{y}_1^{[k]}(v), \dots, \boldsymbol{y}_N^{[k]}(v)] \in \mathbb{R}^N$, where $\boldsymbol{y}^{[k]}(v) = \boldsymbol{W}^{[k]} \boldsymbol{x}^{[k]}(v)$.

One approach to solve this problem in JBSS algorithms is to assume source dependence across the different datasets, i.e., sources of the same index n present dependencies across the K datasets forming N sets of K sources. IVA models this dependence by defining the concept of "source component vector (SCV)", and JBSS methods perform the separation by either maximizing dependence within these SCVs and/or minimizing dependence among the different SCVs. Each of the N latent SCVs is denoted as $\boldsymbol{s}_n = [s_n^{[1]}, \dots, s_n^{[K]}]^\top \in \mathbb{R}^K$, and the estimated SCVs as $\boldsymbol{y}_n = [y_n^{[1]}, \dots, y_n^{[K]}]^\top \in \mathbb{R}^K$. For multi-subject fMRI analysis, where the K datasets correspond to K subjects, the SCV represents the concatenation of K sources that represent similar brain regions for the K subjects.

III. METHODOLOGY

A. Independent Vector Analysis (IVA)

Assuming the latent SCVs are independent, the goal of IVA is to minimize the mutual information among the estimated SCVs $\boldsymbol{y}_n$, thus, maximizing the independence between the N SCVs. For this purpose, IVA models each SCV with a multidimensional probability density function (PDF), allowing it to exploit the statistical dependencies across the datasets. The IVA cost function is given as [5], [7]

$$\mathcal{J}_{\text{IVA}}(\mathcal{W}) = \sum_{n=1}^{N} \left(\sum_{k=1}^{K} \mathcal{H}(\boldsymbol{y}_n^{[k]}) - \mathcal{I}(\boldsymbol{y}_n) \right) - \sum_{k=1}^{K} \log |\det(\boldsymbol{W}^{[k]})|,$$

where $\mathcal{W} = \{\boldsymbol{W}^{[k]}\}_{k=1}^{K}$, $\mathcal{H}(\boldsymbol{y}_n^{[k]})$ denotes the entropy of the nth source estimate for the kth dataset and $\mathcal{I}(\boldsymbol{y}_n)$ denotes the mutual information of the nth SCV. Therefore, we can appreciate that the cost function simultaneously maximizes the independence within a dataset with the entropy term and also maximizes dependence across datasets by maximizing the mutual information of the SCVs.

Different approaches have been implemented to model the PDF of the SCVs [7], [11]. Multivariate Gaussian distribution (MGD) has proven to be an efficient and effective solution for modeling the SCVs. In this case, the IVA algorithm, i.e., IVA-G [7], [17], only exploits second-order statistics and thus minimizes the correlation between different SCVs and maximizes the correlation within each SCV. The PDF of each SCV is given by $p(\boldsymbol{y}_n | \boldsymbol{\Sigma}_{\boldsymbol{y}_n}) = \frac{1}{(2\pi)^{\frac{K}{2}} \det(\boldsymbol{\Sigma}_{\boldsymbol{y}_n})^{\frac{1}{2}}} \exp(-\frac{1}{2} \boldsymbol{y}_n^\top \boldsymbol{\Sigma}_n^{-1} \boldsymbol{y}_n)$,

where $\mathbf{\Sigma}_{\boldsymbol{y}_n} \in \mathbb{R}^{K\times K}$ is the covariance matrix of the nth estimated SCV. Thus, the IVA-G cost function is defined as

$$\mathcal{J}_{\text{IVA-G}}(\mathcal{W}) = \frac{NK\log(2\pi e)}{2} + \frac{1}{2}\sum_{n=1}^{N}\log|\det(\mathbf{\Sigma}_{\boldsymbol{y}_n})| - \sum_{k=1}^{K}\log|\det(\boldsymbol{W}^{[k]})|. \tag{2}$$

The SCVs corresponding to fMRI data represent brain regions that have multivariate heavy-tailed distributions, and therefore super-Gaussian distributions, such as the multivariate Laplacian, provide better model match with the latent fMRI sources [11]. However, this approach is computationally expensive since its iteration complexity depends on the number of data samples. Thus, in this work, we incorporate reference signals into the IVA-G decomposition to guide the estimation and maintain the model match while providing a computationally efficient solution [18].

B. Constrained IVA

cIVA techniques incorporate prior information about the sources into the IVA model [19] in order to guide the decomposition and limit the solution space. Consider a set of references $\{\boldsymbol{r}_n\}_{n=1}^{M} \subset \mathbb{R}^V (M \leq N)$, the objective is to maximize the similarity between $\boldsymbol{r}_n$ and the corresponding estimated SCV $\boldsymbol{y}_n$ while also minimizing similarity with the other estimated SCV $\boldsymbol{y}_m$ where $n \neq m$. For this purpose, the following regularization term is defined as in [18]

$$\mathcal{J}_{\text{ref}}(\mathcal{W}) = \sum_{n=1}^{M}\sum_{k=1}^{K}\left(\sum_{\substack{m=1\\m\neq n}}^{M}\epsilon^2(\boldsymbol{r}_n, \boldsymbol{y}_m^{[k]}) - \epsilon^2(\boldsymbol{r}_n, \boldsymbol{y}_n^{[k]})\right), \tag{3}$$

where $\epsilon : \mathbb{R}^V \times \mathbb{R}^V \to [0,1]$ is implemented as the absolute value of the Pearson correlation.

The augmented cost function is a linear combination of the IVA-G cost function and the regularization term

$$\mathcal{L}_\lambda(\mathcal{W}) = \mathcal{J}_{\text{IVA-G}}(\mathcal{W}) + \frac{\lambda}{2}\mathcal{J}_{\text{ref}}(\mathcal{W}), \tag{4}$$

where λ is a regularization parameter that weights the influence of the IVA-G cost and the regularization term in the final cost function. In this work, after an empirical study for different λ values, we decided to set $\lambda = 5$ as the value that provides a fair trade-off between both terms of the cost.

C. Cross-joint-ISI

Intersymbol interference (ISI) is a widely used global metric to evaluate BSS techniques when the ground truth is available. Joint ISI, an extension of the normalized ISI, is defined as [7]

$$\text{joint-ISI} = (\boldsymbol{G}^{[1]}, \ldots, \boldsymbol{G}^{[K]}) = \text{ISI}\Big(\frac{1}{K}\sum_{k=1}^{K}|\boldsymbol{G}^{[k]}|\Big), \tag{5}$$

where

$$\text{ISI}(\boldsymbol{G}) = \frac{\sum_{i=1}^{N}\Big(\frac{\sum_{j=1}^{N}G_{ij}}{\max_p G_{ip}} - 1\Big) + \sum_{j=1}^{N}\Big(\frac{\sum_{i=1}^{N}G_{ij}}{\max_p G_{pj}} - 1\Big)}{2N(N-1)},$$

where $\boldsymbol{G}^{[k]} = \boldsymbol{A}^{[k]}\boldsymbol{W}^{[k]}$ with elements denoted as G_{nm}. In the ideal scenario of a perfect separation of the sources, $\boldsymbol{G}$ is an identity matrix subject to permutation and scaling ambiguities, thus achieving zero joint-ISI.

However, in practical scenarios, the ground truth is unknown. Cross-joint ISI, a global metric inspired by join-ISI, is proposed to measure the consistency of the estimated components across R runs when there is no ground truth available. It is defined as cross-joint-ISI$_{ij}(\{\boldsymbol{W}_r^{[k]}\}_{r=1,k=1}^{R,K}) =$ joint-ISI$(\boldsymbol{P}_{i,j}^{[1]}, \ldots, \boldsymbol{P}_{i,j}^{[K]})$, where $\boldsymbol{P}_{i,j}^{[k]} = \boldsymbol{A}_i^{[k]}\boldsymbol{W}_j^{[k]}$, $\boldsymbol{A}_i^{[k]} = (\boldsymbol{W}_i^{[k]})^{-1}$ is the inverse of the kth demixing matrix of the ith run, and $\boldsymbol{W}_j^{[k]}$ is the kth demixing matrix of the jth run. The cross-joint-ISI of the ith run is computed by averaging all it pairwise cross-joint-ISI values:

$$\text{cross-joint-ISI}_i = \frac{1}{R}\sum_{j=1, j\neq i}^{R}\text{cross-joint-ISI}_{ij}. \tag{6}$$

D. Normalized Mutual Information

Since IVA maximizes independence among the latent SCVs, we evaluate the performance of the algorithm by quantifying the mutual information (MI) between the estimated sources [20]. A lower MI would imply a higher independence of the estimated components and therefore a better separation of the latent sources. We compute the pairwise normalized MI (I_{norm}) between two estimates as [21]

$$\mathcal{I}_{\text{norm}}(\boldsymbol{y}_i, \boldsymbol{y}_j) = \frac{2I(\boldsymbol{y}_i, \boldsymbol{y}_j)}{I(\boldsymbol{y}_i, \boldsymbol{y}_i) + I(\boldsymbol{y}_j, \boldsymbol{y}_j)}, \tag{7}$$

where $I(\boldsymbol{y}_i, \boldsymbol{y}_j)$ is the mutual information between two estimated components $\boldsymbol{y}_i$ and $\boldsymbol{y}_j$. For each run of the algorithm, we first calculate the pairwise mutual information between all N sources within each subject's dataset and average these $N(N-1)/2$ pairs MI values. Then, the average across all datasets is obtained and used as a metric to describe the performance of the JBSS algorithm in that specific run. The averaged normalized MI (N-MI) for the rth run is obtained as

$$\text{N-MI}_r = \frac{2}{KN(N-1)}\sum_{k=1}^{K}\sum_{i=1}^{N}\sum_{j>i}^{N}\mathcal{I}_{\text{norm}}(\boldsymbol{y}_i^{[k]}, \boldsymbol{y}_j^{[k]}), \tag{8}$$

where $\boldsymbol{y}_i^{[k]}$ and $\boldsymbol{y}_j^{[k]}$ are the source estimates of the kth subject.

IV. Experimental Results

A. Resting-state fMRI data

We use the resting state fMRI data set from the bipolar-schizophrenia network on intermediate phenotypes (B-SNIP) [22]. We employ the data collected from the Baltimore site and select $K = 98$ subjects: 49 healthy controls (HCs) and 49 randomly selected schizophrenia patients (SZs). A single 5-minute run with open eyes consisting of 134 time points was captured for each subject. We removed the first 3 time points to address the T-1 effect. The data were resampled to $3 \times 3 \times 3$ mm^3 isotropic voxels. In addition, to remove non-brain voxels and flatten the data, each subject image was masked, yielding an observation vector of $V = 50223$ voxels for each of the $T = 131$ time points.

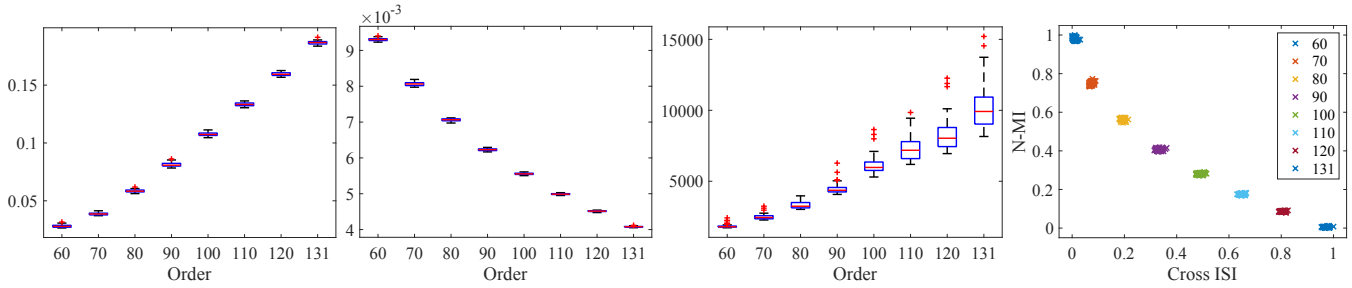

(a) Cross-joint-ISI (b) N-MI (c) Runtime (seconds) (d) N-MI vs. cross-joint-ISI

Fig. 1: Comparison of different model orders for real fMRI data with $K = 98$ and $V = 50223$. The (a) cross-joint-ISI, (b) normalized mutual information, and (c) runtime, are shown for 50 independent runs as functions of the number of components N. Figure (d) shows the reproducibility vs accuracy plot. Both cross-joint-ISI and N-MI were rescaled with the min/max scaler for better visualization. Each of the markers of the plot represents one independent run.

B. Results

We evaluate the performance of the cIVA-G algorithm in terms of reproducibility and accuracy metrics as a function of the model complexity. For this purpose, different model orders are analyzed when applied to real fMRI data. In these experiments, we use the functional templates extracted by Neuromark, specifically the neuromark_fMRI_1.0 template [3], which is composed of 53 resting-state networks (RSNs) from seven different functional domains: SC (5 RSNs), AUD (2 RSNs), MOT (9 RSNs), VIS (9 RSNs), CC (17 RSNs), DMN (7 RSNs) and CB (4 RSNs). Each of these RSNs is employed as a reference signal by the algorithm for all the model orders tested, i.e., $M = 53$ for all the experiments. However, the number of components to estimate is always higher than the number of references $N > M$, ranging from $60 \leq N \leq 131$.

The obtained results of 50 independent runs for each of the tested model orders are shown in Fig. 1. The cross-joint-ISI values are depicted in Fig. 1-a. As can be appreciated, there is a direct relation between model order and cross-joint-ISI values, as the order increases, the cross-joint-ISI values also increase. cIVA-G requires the estimation of high-dimensional probability density functions and the parameters for the demixing matrices. Therefore, for a fixed number of samples V, the performance of the algorithm degrades in terms of cross-joint-ISI with the increase in the number of components N or the number of datasets K [11], [12]. Thus, a higher model complexity leads to larger variance and lower reproducibility of the results. The same pattern can be appreciated in the runtime on Fig. 1-c. On the other hand, N-MI values show the opposite behavior (see Fig. 1-b), where the higher the model complexity, the lower the N-MI. In this case, the inclusion of more information into the analysis by incrementing the number of components helps the algorithm to better separate the estimated sources and make them more statistically independent. Therefore, from these results, we can appreciate the classic bias-variance tradeoff, as illustrated in Fig. 1-d. Thus, an adequate model order will be the one that finds a balance between these two aspects: accuracy (independence in our problem) and reproducibility. We can see that the model orders 90 and 100 are the ones that better balance this tradeoff between the cross-joint-ISI and N-MI values.

To determine the final model order, we analyze the quality of the estimation and the interpretability of the results obtained by these model complexities. One important metric to assess the interpretability of the results is the power spectra of RSN time courses and the power ratio between low-frequency (< 0.1 Hz) and high-frequency (> 0.15 Hz) bands. Low-frequency activity is usually related to BOLD signals, therefore a high power ratio value is associated with brain activity, while low power ratio values are related to respiratory or cardiac activity [23]. To calculate this ratio, we select the run that offers the lowest combination of cross-joint-ISI and N-MI for each order. The Euclidean distance from the origin $(0, 0)$ to the point defined by the cross-joint-ISI and the N-MI of each run is calculated and the run with the minimum distance is selected. To give both metrics the same weight in this selection, a min/max scaling of both metrics is performed to rescale the values to the interval $[0, 1]$. The average power ratio is calculated for the 53 components related to the references. Model order 60 obtains a value of 3.74 ± 2, model order 90 offers a power ratio of 3.92 ± 2.54, model order 100 of 4 ± 2.82, and model order 120 of 3.97 ± 2.83. From these results, we can appreciate that for the model orders that balance the tradeoff between N-MI and cross-joint-ISI, such as model order 100, there is a better model match than for those that minimize the cross-joint-ISI, such as model order 60. Fig. 2 shows the spatial maps of two estimated components for model order 60 and 100 as an example. We can see that order 100 presents more interpretable results, with clearer maps and more focal activation areas.

The functional network connectivity (FNC) map shows the correlation of the time courses between components. We expect the components within a functional domain to present higher connectivity values [23]. In Fig. 3 we can observe that order 100 shows larger correlations given a functional domain, while for order 60 the connectivity values are weaker. These

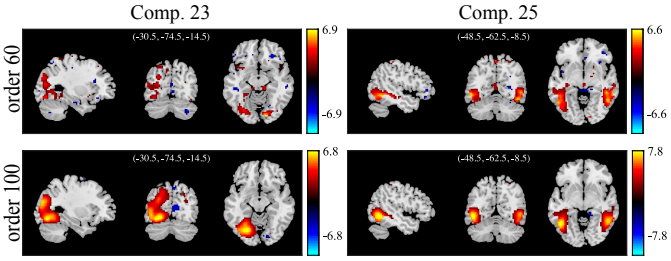

Fig. 2: Spatial maps for two estimated components for two different model orders: 60 and 100.

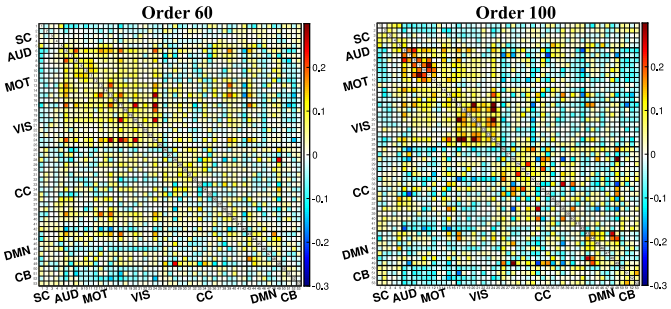

Fig. 3: Average FNC matrix. Pairwise Pearson correlation between estimated RSNs time courses are first Fisher z-transformed and averaged across all subjects. Only the 53 RSNs related to the references are analyzed.

results suggest again that order 100 offers a better model match for fMRI data and more interpretable results.

V. Conclusions

We presented a new mechanism for selecting the best model order for a JBSS technique, such as constrained IVA. For this purpose, we employed cross-joint-ISI and normalized pairwise mutual information of the estimated sources to evaluate the reproducibility and the accuracy of the results. The results obtained with real fMRI data show that the model order that balances the tradeoff between both metrics achieves a better model match with higher quality estimates and more interpretable results. Future work will study if the two metrics contribute the same to the quality of the results, or whether one of them should have more weight than the other in the order selection.

References

[1] R. A. Poldrack and K. J. Gorgolewski, "Making big data open: data sharing in neuroimaging," *Nat. Neurosci.*, vol. 17, no. 11, pp. 1510–1517, 2014.

[2] V. D. Calhoun and T. Adalı, "Multisubject independent component analysis of fMRI: A decade of intrinsic networks, default mode, and neurodiagnostic discovery," *IEEE Trans. Biomed. Eng.*, vol. 5, pp. 60–73, 2012.

[3] Y. Du, Z. Fu, J. Sui, S. Gao, Y. Xing, D. Lin, M. Salman, A. Abrol, M. A. Rahaman, J. Chen *et al.*, "NeuroMark: An automated and adaptive ICA based pipeline to identify reproducible fMRI markers of brain disorders," *NeuroImage Clin.*, vol. 28, p. 102375, 2020.

[4] M. J. McKeown, S. Makeig, G. G. Brown, T.-P. Jung, S. S. Kindermann, A. J. Bell, and T. J. Sejnowski, "Analysis of fMRI data by blind separation into independent spatial components," *Hum. Brain Mapp.*, vol. 6, no. 3, pp. 160–188, 1998.

[5] T. Adalı, M. Anderson, and G.-S. Fu, "Diversity in independent component and vector analyses: Identifiability, algorithms, and applications in medical imaging," *IEEE Signal Process. Mag.*, vol. 31, no. 3, pp. 18–33, 2014.

[6] V. D. Calhoun, T. Adalı, G. D. Pearlson, and J. J. Pekar, "A method for making group inferences from functional MRI data using independent component analysis," *Hum. Brain Mapp.*, vol. 14, no. 3, pp. 140–151, 2001.

[7] M. Anderson, T. Adalı, and X.-L. Li, "Joint blind source separation with multivariate Gaussian model: Algorithms and performance analysis," *IEEE Trans. Signal Process.*, vol. 60, no. 4, pp. 1672–1683, 2011.

[8] A. M. Michael, M. Anderson, R. L. Miller, T. Adalı, and V. D. Calhoun, "Preserving subject variability in group fMRI analysis: Performance evaluation of GICA vs. IVA," *Front. Syst. Neurosci.*, vol. 8, p. 106, 2014.

[9] T. Kim, T. Eltoft, and T.-W. Lee, "Independent vector analysis: An extension of ICA to multivariate components," in *Independent Component Analysis and Blind Signal Separation*. Springer, 2006, pp. 165–172.

[10] E. A. Allen, E. B. Erhardt, Y. Wei, T. Eichele, and V. D. Calhoun, "Capturing inter-subject variability with group independent component analysis of fMRI data: a simulation study," *Neuroimage*, vol. 59, no. 4, pp. 4141–4159, 2012.

[11] S. Bhinge, R. Mowakeaa, V. D. Calhoun, and T. Adalı, "Extraction of time-varying spatiotemporal networks using parameter-tuned constrained IVA," *IEEE Trans. Med. Imag.*, vol. 38, no. 7, pp. 1715–1725, 2019.

[12] Q. Long, S. Bhinge, V. D. Calhoun, and T. Adalı, "Independent vector analysis for common subspace analysis: Application to multi-subject fMRI data yields meaningful subgroups of schizophrenia," *NeuroImage*, vol. 216, p. 116872, 2020.

[13] T. Adali, F. Kantar, M. A. B. S. Akhonda, S. Strother, V. D. Calhoun, and E. Acar, "Reproducibility in matrix and tensor decompositions: focus on model match, interpretability, and uniqueness," *IEEE Signal Process. Mag.*, vol. 39, no. 4, pp. 8–24, 2022.

[14] T. Adali and V. D. Calhoun, "Reproducibility and replicability in neuroimaging data analysis," *Curr. Opin. Neurol.*, vol. 35, no. 4, pp. 475–481, 2022.

[15] Q. Long, C. Jia, Z. Boukouvalas, B. Gabrielson, D. Emge, and T. Adalı, "Consistent run selection for independent component analysis: Application to fMRI analysis," in *Proc. IEEE Int. Conf. Acoust. Speech Signal Process.* IEEE, 2018, pp. 2581–2585.

[16] S. C. Strother, J. Anderson, L. K. Hansen, U. Kjems, R. Kustra, J. Sidtis, S. Frutiger, S. Muley, S. LaConte, and D. Rottenberg, "The quantitative evaluation of functional neuroimaging experiments: the NPAIRS data analysis framework," *NeuroImage*, vol. 15, no. 4, pp. 747–771, 2002.

[17] M. Anderson, G.-S. Fu, R. Phlypo, and T. Adalı, "Independent vector analysis: Identification conditions and performance bounds," *IEEE Trans. Signal Process.*, vol. 62, no. 17, pp. 4399–4410, 2014.

[18] T. Vu, F. Laport, H. Yang, V. D. Calhoun, and T. Adali, "Constrained independent vector analysis with reference for multi-subject fMRI analysis," *arXiv preprint arXiv:2311.05049*, 2023.

[19] S. Bhinge, Q. Long, Y. Levin-Schwartz, Z. Boukouvalas, V. D. Calhoun, and T. Adalı, "Non-orthogonal constrained independent vector analysis: Application to data fusion," in *Proc. IEEE Int. Conf. Acoust. Speech Signal Process.* IEEE, 2017, pp. 2666–2670.

[20] M. Sun, B. Gabrielson, M. A. B. S. Akhonda, H. Yang, F. Laport, V. Calhoun, and T. Adali, "A scalable approach to independent vector analysis by shared subspace separation for multi-subject fMRI analysis," *Sensors*, vol. 23, no. 11, p. 5333, 2023.

[21] Q. Long, S. Bhinge, Y. Levin-Schwartz, Z. Boukouvalas, V. D. Calhoun, and T. Adalı, "The role of diversity in data-driven analysis of multi-subject fMRI data: Comparison of approaches based on independence and sparsity using global performance metrics," *Human Brain Mapping*, vol. 40, no. 2, pp. 489–504, 2019.

[22] C. A. Tamminga, E. I. Ivleva, M. S. Keshavan, G. D. Pearlson, B. A. Clementz, B. Witte, D. W. Morris, J. Bishop, G. K. Thaker, and J. A. Sweeney, "Clinical phenotypes of psychosis in the bipolar-schizophrenia network on intermediate phenotypes (B-SNIP)," *Am. J. Psychiatry*, vol. 170, no. 11, pp. 1263–1274, 2013.

[23] E. A. Allen, E. B. Erhardt, E. Damaraju, W. Gruner, J. M. Segall, R. F. Silva, M. Havlicek, S. Rachakonda, J. Fries, R. Kalyanam *et al.*, "A baseline for the multivariate comparison of resting-state networks," *Front. Syst. Neurosci.*, vol. 5, p. 2, 2011.